TISSUE ENGINEERING: Part A
Volume 14, Number 00, 2008

DOI: 10.1089/ten.tea.2008.0014

Novel Nanofiber-Based Scaffold for Rotator Cuff Repair and Augmentation

Kristen L. Moffat, M.S.,[1] Anne S.-P. Kwei,[1] Jeffrey P. Spalazzi, Ph.D.,[1] Stephen B. Doty, Ph.D.,[2] William N. Levine, M.D.,[3] and Helen H. Lu, Ph.D.[1,4]

The debilitating effects of rotator cuff tears and the high incidence of failure associated with current grafts underscore the clinical demand for functional solutions for tendon repair and augmentation. To address this challenge, we have designed a poly(lactide-*co*-glycolide) (PLGA) nanofiber-based scaffold for rotator cuff tendon tissue engineering. In addition to scaffold design and characterization, the objective of this study was to evaluate the attachment, alignment, gene expression, and matrix elaboration of human rotator cuff fibroblasts on aligned and unaligned PLGA nanofiber scaffolds. Additionally, the effects of *in vitro* culture on scaffold mechanical properties were determined over time. It has been hypothesized that nanofiber organization regulates cellular response and scaffold properties. It was observed that rotator cuff fibroblasts cultured on the aligned scaffolds attached along the nanofiber long axis, whereas the cells on the unaligned scaffold were polygonal and randomly oriented. Moreover, distinct integrin expression profiles on these two substrates were observed. Quantitative analysis revealed that cell alignment, distribution, and matrix deposition conformed to nanofiber organization and that the observed differences were maintained over time. Mechanical properties of the aligned nanofiber scaffolds were significantly higher than those of the unaligned, and although the scaffolds degraded *in vitro*, physiologically relevant mechanical properties were maintained. These observations demonstrate the potential of the PLGA nanofiber-based scaffold system for functional rotator cuff repair. Moreover, nanofiber organization has a profound effect on cellular response and matrix properties, and it is a critical parameter for scaffold design.

Introduction

The rotator cuff consists of four muscles and tendons, including the supraspinatus, infraspinatus, teres minor and subscapularis, which function in synchrony to stabilize the glenohumeral joint and actively control shoulder kinematics. Rotator cuff tears are among the most common injuries afflicting the shoulder, with more than 75,000 repair procedures performed annually in the United States alone.[1] Clinical intervention is required, since rotator cuff injuries do not heal due to the complex anatomy and extended range of motion of the shoulder joint, as well as the relative weakening and hypovascularization of the cuff tendons post-injury.[2–4]

Due to the high failure rates associated with current repair procedures, coupled with the clinical need to treat large tears and chronic cuff degeneration, a significant demand exists for a functional rotator cuff grafting system. For example, failure rates as high as 94% have been reported after primary repair of chronic cuff injuries,[5] generally attributed to factors such as osteoporotic bone, degenerative and poorly vascularized tendons, severe tendon weakening, muscle atrophy, and size of the original defect.[6–8] Moreover, surgical repair often results in excessive tension on the cuff tissues at the repair site.[9,10] Although the use of synthetic tendon grafts have been reported,[11,12] poor biocompatibility and insufficient mechanical strength have rendered these grafts suboptimal for rotator cuff repair.

Recently, biological grafts based on allogeneic and xenogeneic extracellular matrices have been considered for cuff repair and augmentation.[4,13] Collagen-rich dermis and small intestinal submucosa (SIS)[14] have been marketed commercially as graft patches for reinforcing cuff repair.[15,16] With its biomimetic, collagen nanofiber-based architecture and alignment, SIS is particularly attractive because it can be readily remodeled by host cells, while encouraging angiogenesis and neo-collagen production.[14] Although promising results have been reported in animal models,[4,13] augmentation with SIS

[1]Biomaterials and Interface Tissue Engineering Laboratory, Department of Biomedical Engineering, Columbia University, New York, New York.
[2]Analytical Microscopy Laboratory, Hospital for Special Surgery, New York, New York.
[3]Department of Orthopedic Surgery, Columbia University Medical Center, New York, New York.
[4]College of Dental Medicine, Columbia University Medical Center, New York, New York.

did not improve the rate of tendon healing in human trials.[16] Recently, using a canine model, Derwin *et al.*[15] conducted a systematic comparison of the biomechanical properties of four commercially available extracellular matrices for rotator cuff augmentation. Significantly lower mechanical properties than those of the infraspinatus tendon were observed in all grafts tested, and the mechanical properties of SIS decreased due to premature resorption.[15] Similar outcomes have been reported for other biological grafts.[17,18] Therefore, despite their apparent structural advantages, the suboptimal clinical outcomes of biologically derived grafts may be attributed to inferior mechanical properties, the mismatch in kinetics of graft remodeling, and the rate of neo-matrix production.

The debilitating effect of rotator cuff tears, coupled with the high incidence of failure associated with existing graft choices, underscore the clinical need for alternative grafting solutions. Our long-term objective is to engineer biomimetic, functional, and integrative scaffold systems for rotator cuff repair and augmentation. The ideal scaffold for rotator cuff tendon repair must be able to meet the physiologic demand of the native tendon by matching its mechanical properties, and it should promote host cell–mediated healing by mimicking the ultrastructural organization of the native tendon. In addition, the scaffold should be biodegradable so that new tissue can replace it gradually while physiologically relevant mechanical properties are maintained. Finally, the scaffold must be able to integrate with the host tendon and surrounding bone tissue. This study, guided by these design criteria, evaluated the potential of a degradable nanofiber-based scaffold system for rotator cuff repair. Nanofibers are advantageous for tendon tissue engineering because of their superior biomimetic potential and physiological relevance. They have been investigated with promising results for bone,[19,20] meniscus,[21] intervertebral disk,[22] cartilage,[23] and ligament[24,25] tissue engineering. A distinct advantage of nanofiber scaffolds is that they can be engineered to resemble the native tendon extracellular matrix, and designed to exhibit high aspect ratio, surface area, permeability, and porosity.[26–31] Moreover, nanofiber organization and alignment can be modulated during fabrication,[31,32] which allows for scaffold structural and material properties to be readily tailored to meet the functional demands of the rotator cuff tendons.

Specifically, this study focused on the design, characterization, and *in vitro* evaluation of a poly(D,L-lactide-*co*-glycolide)-based nanofiber scaffold for rotator cuff repair. The effects of nanofiber organization (aligned vs unaligned) on the attachment, gene expression, and matrix deposition of human rotator cuff fibroblasts were determined over time. The three study objectives were first to characterize the structural and mechanical properties of aligned and unaligned nanofiber scaffolds, then to evaluate the effects of fiber organization (aligned vs unaligned) on the response of human rotator cuff fibroblasts, and finally, to examine the effects of *in vitro* fibroblast culture on the mechanical properties of the tissue-engineered scaffolds. The nanofiber scaffold is designed to match the structural and mechanical properties of the rotator cuff tendon, and it is hypothesized that the underlying nanofiber organization will guide fibroblast attachment, morphology, and matrix elaboration. This is the first reported study on the application of tissue engineering for rotator cuff regeneration using biomimetic, nanofiber-based scaffolds, and it is anticipated that this scaffold will serve as a promising grafting system for functional rotator cuff repair and augmentation.

Materials and Methods

Nanofiber scaffold fabrication

Nanofiber scaffolds (Fig. 1) based on poly(D,L-lactide-*co*-glycolide) 85:15 co-polymer (PLGA, $M_w \approx 123.6$ kDa; Lakeshore Biomaterials, Birmingham, AL) were produced using electrospinning.[33–35] Briefly, a 35% (v/v) solution of PLGA was mixed with 55% N,N-dimethylformamide (Sigma-Aldrich, St. Louis, MO) and 10% ethyl alcohol. The polymer solution was loaded into a 5-mL syringe with a 18.5-gauge stainless steel blunt-tip needle and electrospun at 8 to 10 kV using a custom electrospinning device. To fabricate unaligned nanofiber scaffolds, the collecting surface consisted of a stationary plate, and a custom rotating mandrel (20 m/s) was used to produce aligned scaffolds. The polymer solution was dispensed using a syringe pump (Harvard Apparatus, Holliston, MA; 1 mL/h).

Nanofiber scaffold characterization

The structural and material properties of the nanofiber scaffolds were characterized post-fabrication. Specifically, nanofiber morphology and organization were imaged using scanning electron microscopy (SEM, 5 kV, FEI Quanta 600, FEI Co. Hillsboro, OR). For SEM analysis, the scaffolds were sputter-coated with palladium to reduce charging effects. Fiber diameter was quantified using image analysis of SEM micrographs (2000×, $n = 5$ images/group, ImageJ, National Institutes of Health, Bethesda, MD). In addition, scaffold porosity and pore diameter ($n = 5$/group) were evaluated using mercury porosimetry (Micromeritics Autopore III, Norcross, GA) following published protocols,[36] in which porosity was determined by measuring the volume of mercury infused into the sample. Scaffold permeability ($n = 5$/group) was determined by measuring the pressure difference across the scaffold with a custom device[37,38] and then calculating permeability according to Darcy's Law.

The mechanical properties of the as-fabricated aligned and unaligned nanofiber scaffolds were evaluated under uniaxial tensile testing.[39] Briefly, the scaffolds (6 cm × 1 cm, $n = 5$/group) were secured with custom clamps and mounted on a mechanical testing device (Instron, Model 8841, Norwood, MA) with an average gauge length of 3 cm. The samples were evaluated to failure at a strain rate of 5 mm/min, with the aligned scaffolds tested along the nanofiber long axis. Scaffold yield strength and ultimate tensile stress were determined, and elastic modulus was calculated from the linear region of the stress-strain curve.

In vitro *culture of human rotator cuff fibroblasts on nanofiber scaffolds*

Cells and cell culture. Human rotator cuff fibroblast-like cells were derived from explant culture of tissues obtained from three patients (female, aged 65 to 70 years, institutional review board exempt) undergoing rotator cuff repair surgery. Briefly, the tissue samples were rinsed with phosphate buffered saline (PBS, Sigma-Aldrich), plated in tissue culture dishes, and maintained in Dulbecco's modified Eagle medium supplemented with 10% fetal bovine serum, 1% non-essential

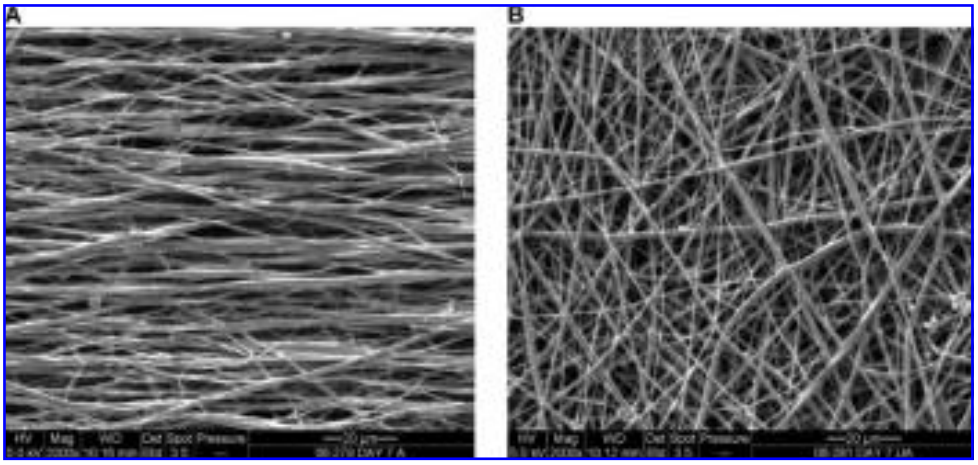

FIG. 1. Aligned and unaligned nanofiber scaffolds. Scanning electron micrographs of (**A**) aligned and (**B**) unaligned scaffolds, 2000×, bar = 20 μm.

amino acids, 1% penicillin/streptomycin, and 1% amphotericin B. The cells from the first migration were subsequently discarded, and the tissue was re-plated in fresh fully supplemented medium. Only cells obtained from the second and third migrations were used in this study, because this method has been shown to yield a relatively homogenous fibroblast population.[39] All medium and supplements were purchased from Mediatech (Herndon, VA).

Cell seeding on nanofiber scaffolds. To prevent scaffold contraction,[40] the nanofiber scaffolds were secured using custom-made clamps. After ultraviolet sterilization, the scaffolds were pre-incubated in fully supplemented medium at 37°C and 5% carbon dioxide for 16 h. Human rotator cuff fibroblasts (passage 4) were seeded on the scaffolds at a density of 3×10^4 cells/cm^2 and allowed to attach for 15 min before the addition of fully supplemented medium. The cells were cultured on the aligned and unaligned nanofiber scaffolds for 2 weeks, with monolayer culture of the human tendon fibroblasts and acellular scaffolds (aligned as well as unaligned) serving as controls. The effects of nanofiber organization on cell morphology, attachment, gene expression, proliferation, and matrix production were determined throughout the 2-week culturing period. In addition, the effects of *in vitro* culture on scaffold mechanical properties were evaluated over time.

Cell viability and attachment morphology

Cell attachment morphology ($n = 3$/group) on the nanofiber scaffolds was evaluated at 1, 7, and 14 days using SEM (FEI Quanta 600). The samples were first rinsed with 0.1 M sodium cacodylate buffer (Sigma-Aldrich), incubated in Karnovsky's fixative[41] for 24 hours at 4°C, and subsequently dehydrated with an ethanol series. In addition, cell viability ($n = 3$/group) and attachment morphology were evaluated using Live/Dead staining (Molecular Probes, Eugene, OR). The samples were rinsed twice with PBS and stained following the manufacturers suggested protocol. The samples were imaged under confocal microscopy (Olympus Fluoview IX70, Center Valley, PA) at wavelengths of 488 nm and 568 nm. To evaluate cell penetration into the scaffold, a z-series of confocal images were collected over a depth of 10 μm, equivalent to 15 to 20 layers of nanofibers.

Quantitative analysis of cell attachment on nanofiber scaffolds

The effects of nanofiber organization (aligned vs unaligned) on fibroblast attachment were quantified at 1, 7, and 14 days following the methods of Costa *et al.*[42] Briefly, confocal images ($n = 3$ images/group) of fibroblast-seeded nanofiber scaffolds and acellular scaffolds were analyzed using circular statistics software customized for evaluating fiber alignment (Fiber3). The circular statistics parameters determined included mean vector angle, which represents the average fiber alignment in the matrix ($-90^\circ \le \theta \le 90^\circ$; 0° indicates horizontal orientation); mean vector length, which ranges from zero for a randomly distributed sample to unity for an aligned sample ($0 \le r \le 1$); and angular deviation, which characterizes the dispersion of the non-Gaussian angle distribution of the nanofibers (0-40.5°). Specifically, an angular deviation of 0° represents an aligned sample, and 40.5° is indicative of random distribution.

Gene expression

Gene expression ($n = 5$/group) was measured using reverse transcriptase polymerase chain reaction (RT-PCR) at 1, 3, and 14 days. Total RNA was isolated using the Trizol extraction method (Invitrogen, Carlsbad, CA). The isolated RNA was reverse-transcribed into complementary DNA (cDNA) using the SuperScript First-Strand Synthesis System (Invitrogen), and the cDNA product was then amplified using recombinant Taq DNA polymerase (Invitrogen). Expression of integrins α2 (sense, 5′-CAGAATTTGGAACGGGACTT-3′; antisense, 5′- CAGGTAGGTCTGCTGGTTCA-3′), α5 (sense, 5′-GTGGCCTTCGGTTTACAGTC-3′; antisense, 5′-AATAGC ACTGCCTCAGGCTT-3′), αV (sense, 5′-GATGGACCAATG AACTGCAC-3′; antisense, 5′-TTGGCAGACAATCTTCAAG C-3′), and β1 (sense, 5′- GAGGAATACAGCCTGTGGGT-3′; antisense, 5′-CAGAAGGTGCAGAGATGATGA-3′) were determined over time. Type I collagen (sense, 5′-TGCTGGC CAACTATGCCTCT-3′; antisense, 5′ TTGCACAATGCTCT GATC-3′) and type III collagen (sense, 5′- CCAAACTCTAT CTGAAATCC-3′; antisense, 5′-GGACTCATAGAATACAAT CT-3′) expression were also examined. Glyceraldehyde-3-phosphate dehydrogenase (GAPDH, sense, 5′- GGCGATGC TGGCGCTGAGTA-3′; antisense, 5′-ATCCACAGTCTTCT

Table 1. Summary of the Structural Properties of Aligned and Unaligned Scaffolds

	Scaffold Thickness (mm)	*Fiber Diameter (nm)*	*Pore Diameter (μm)*	*Porosity (%)*	*Permeability ($m^4/N\,s$)*
Aligned ($n=5$)	0.22 ± 0.02	615 ± 152	4.228 ± 1.056	80.745 ± 2.966	$(7.87 \pm 2.47) \times 10^{-12}$
Unaligned ($n=5$)	0.19 ± 0.02	568 ± 147	4.914 ± 0.777	81.760 ± 3.929	$(5.72 \pm 0.63) \times 10^{-12}$

GGGTGG-3′) served as the house-keeping gene. All genes were amplified for 30 cycles in a thermocycler (Eppendorf Mastercycler gradient, Brinkmann, Westbury, NY). Semi-quantitative analysis of gene expression (ImageJ) was performed, and band intensity was normalized to that of GAPDH.

Cell proliferation

Cell proliferation ($n=5$ samples/group) was determined by measuring total DNA content using the PicoGreen double strand DNA assay (Invitrogen) following the manufacturer's suggested protocol. At designated time points, each scaffold was rinsed with PBS and homogenized in 0.1% Triton X solution (Sigma-Aldrich). Fluorescence was measured using a microplate reader (Tecan, Research Triangle Park, NC) at the excitation and emission wavelengths of 485 nm and 535 nm, respectively. A standard curve was generated to correlate DNA content with fluorescence intensity, and the number of cells was determined using a conversion factor of 8 pg DNA/cell.[39]

Cell matrix production

Fibroblast elaboration of type I and type III collagen ($n=3$ samples/group) on the aligned and unaligned scaffolds was evaluated using immunohistochemistry at 7 and 14 days. After rinsing with PBS, the samples were fixed with 10% neutral buffered formalin for 24 h. Monoclonal antibodies for type I collagen (1:20 dilution) and type III collagen (1:100) were obtained from EMD Chemicals (Calbiochem, San Diego, CA) and Sigma-Aldrich, respectively. Before staining for type III collagen, the samples were treated with 1% hyaluronidase for 30 min at 37°C and incubated with primary antibody overnight. After a PBS wash, biotinylated secondary antibody and streptavidin conjugate (LSAB2 System-HRP, DakoCytomation, Carpinteria, CA) were added. The formation of red-brown precipitates indicated positive staining with the colorimetric substrate (AEC Substrate Chromogen, DakoCytomation). At day 7, organization of the type I collagen produced by the human fibroblasts was evaluated using the circular statistics software (Fiber3), as described above.

Mechanical properties of the fibroblast-seeded nanofiber scaffolds

The effects of *in vitro* fibroblast culture on the mechanical properties of the aligned and unaligned scaffolds were determined at 1, 7, and 14 days. The human rotator cuff fibroblasts were seeded at a density of 3×10^4 cells/cm^2 on the scaffold. Aligned and unaligned scaffolds without cells (acellular) served as controls. At each designated time point, the samples were tested to failure under uniaxial tension following the protocol described above for the as-fabricated scaffolds. Specifically, the elastic modulus, yield strength, and ultimate tensile stress of the samples ($n=5$ samples/group) were determined.

Statistical analysis

Results are presented in the form of mean ± standard deviation, with n equal to the number of replicates ($n=5$ for all quantitative analyses, $n=3$ for all qualitative analyses). One-way analysis of variance (ANOVA) was performed to determine the effects of fiber organization on scaffold structural and mechanical properties. Two-way ANOVA was used to determine fiber organization and temporal effects on cell alignment, proliferation, and gene expression. Similarly, the effects of *in vitro* culture and culturing time on scaffold tensile mechanical properties were determined. The Tukey-Kramer post-hoc test was used for all pair-wise comparisons, and significance was attained at $p<0.05$. Statistical analyses were performed with JMP IN (4.0.4, SAS Institute, Inc., Cary, NC).

Results

Characterization of the aligned and unaligned nanofiber scaffolds

The structural properties of the as-fabricated scaffolds are summarized in Table 1. The nanofiber diameter of the aligned scaffolds averaged 615 ± 152 nm, whereas that of the unaligned group measured 568 ± 147 nm, with no significant difference found between the groups. Similarly, scaffold porosity, pore diameter, and permeability were comparable between the aligned and unaligned scaffolds (Table 1). In contrast, the mechanical properties of the as-fabricated aligned and unaligned scaffolds differed significantly (Fig. 2, $p<0.05$). As shown in Figure 2, distinct stress–strain profiles were observed for the aligned and unaligned scaffolds, with significant differences detected in tensile properties. Specifically, the elastic modulus of the aligned scaffold was three times as strong, while both yield strength and ultimate tensile stress were nearly four times higher than those of the unaligned scaffolds (Table 2, $p<0.05$).

Effects of nanofiber organization on fibroblast attachment and alignment

Cell attachment morphology. The attachment morphology and growth of human rotator cuff fibroblasts on aligned and unaligned nanofiber scaffolds were visualized using electron and confocal microscopy. As shown in Figure 3, the fibroblasts attached and assumed distinct morphologies on the two types of nanofiber scaffolds. Specifically, the cells grown on the aligned fibers adopted a phenotypic elongated morphology and were oriented in the direction of the fiber long axis. In contrast, fibroblasts seeded on the unaligned fibers

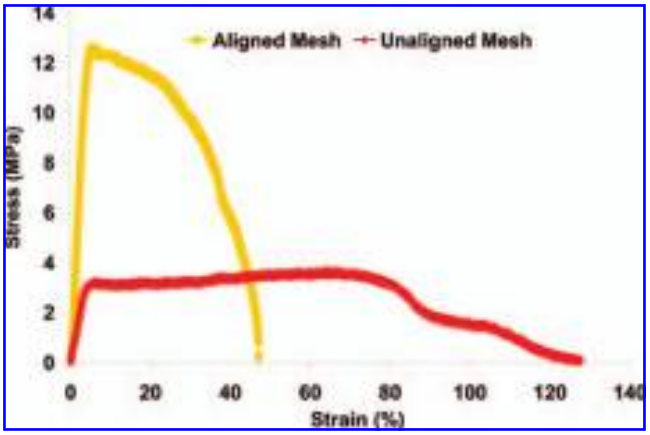

FIG. 2. Mechanical properties of nanofiber scaffolds. A representative stress–strain curve for aligned and unaligned scaffolds tested in uniaxial tension is shown. Color images available online at www.liebertonline.com/ten.

exhibited a polygonal morphology without preferential orientation. Moreover, as fibroblasts proliferated on both types of substrates, these morphological differences were maintained over the 2-week culturing period (Fig. 3).

Gene expression. The expression of integrins and type I and type III collagen were compared over time on the aligned and unaligned scaffolds (Fig. 4). α5 expression did not vary significantly between the nanofiber scaffolds, and no apparent change was observed over time (Fig. 4A). α2 expression (Fig. 4B) differed significantly between the two types of nanofiber scaffolds, with 15, 9, and 10 times greater expression detected in the aligned than in the unaligned group at 1, 7, and 14 days, respectively. After 2 weeks of culture, significantly higher αV expression was seen on the unaligned scaffold (Fig. 4C). Although the expression of β1 (Fig. 4D) was similar between the two scaffold groups, it increased significantly over time, with higher expression ($p < 0.05$) detected at day 14 than on day 1 and day 3. Expression of type I collagen was evident by day 3, whereas type III collagen expression was maintained on aligned and unaligned scaffolds at all time points examined (Fig. 4A). All genes evaluated were also consistently detected in the monolayer control (data not shown).

Quantitative analysis of cell attachment and alignment. The attachment response of human rotator cuff fibroblasts to the inherent organization of the nanofiber scaffolds (aligned vs unaligned) was quantified using circular statistical analysis.[42,43] Specifically, cell alignment and orientation over time were compared with those of the underlying nanofiber substrate, focusing on mean vector angle and angular deviation (Fig. 5A, Table 3) and mean vector length (Fig. 5B). Fibroblasts cultured on the aligned scaffolds were oriented horizontally at day 1, exhibiting similar mean angle distribution (cells: 4.24°, fibers: 4.32°) and narrow angular deviation (cells: 19.73°, fibers: 17.00°) to that of the underlying aligned nanofiber substrate. Fibroblasts on unaligned scaffolds also conformed to matrix organization at day 1, demonstrating a random orientation (cells: −63.46°, fibers: −55.69°) with a wide angular deviation approximating those of the unaligned scaffold matrix (cells: 37.70°, fibers: 35.97°). At day 14, the underlying nanofiber organization continued to dictate fibroblast growth and morphology, with significantly greater alignment measured for fibroblasts cultured on the aligned scaffolds than for those found on the unaligned scaffolds (Fig. 5B, $p < 0.05$). For each scaffold type (aligned or unaligned), circular statistical analysis of fibroblast response revealed no significant change in alignment parameters (mean angle, angular deviation, mean vector length) from the day 1 results.

Effects of nanofiber organization on fibroblast growth and matrix deposition

Tendon fibroblasts proliferated on the nanofiber scaffolds over the 2-week culturing period, with no significant difference in cell growth found between the aligned and unaligned groups (Fig. 6A). Matrix deposition by human fibroblasts on the nanofiber scaffolds was also evaluated over time, and the cells produced a collagen-rich matrix containing type I and type III collagen (Fig. 6B). Additionally, circular statistical analysis of the type I collagen immunohistochemistry images revealed an oriented collagen matrix on the aligned nanofiber scaffold (Fig. 6C), with a mean angle ± angular deviation of 9.08° ± 30.04° and a mean vector length of 0.45. In contrast, a randomly oriented collagen matrix with a mean angle ± angular deviation of −12.04° ± 34.37° and a mean vector length of 0.28 was observed on the unaligned scaffolds.

Effects of in vitro *culture on scaffold mechanical properties*

The mechanical properties of fibroblast-seeded PLGA nanofiber scaffolds were determined over time and compared as a function of cell culture (cellular vs acellular), culturing time, and nanofiber organization (aligned vs unaligned). As expected for PLGA, *in vitro* culture decreased scaffold mechanical properties, with significantly lower ultimate tensile stress and yield strength over time for aligned and unaligned scaffolds than for the as-fabricated scaffolds (Figs. 7A, C; $p < 0.05$). In contrast, *in vitro* culture had no significant effect on scaffold elastic modulus (Fig. 7B). The ultimate tensile stress, elastic modulus, and yield strength of the

Table 2. Summary of the Mechanical Properties of Aligned and Unaligned Scaffolds

	Elastic Modulus (MPa)	*Yield Strength (MPa)*	*Ultimate Stress (MPa)*
Aligned (n = 5)	341 ± 30*	9.8 ± 1.1*	12.0 ± 1.5*
Unaligned (n = 5)	107 ± 23	2.5 ± 0.4	3.7 ± 0.2

*$p < 0.05$.

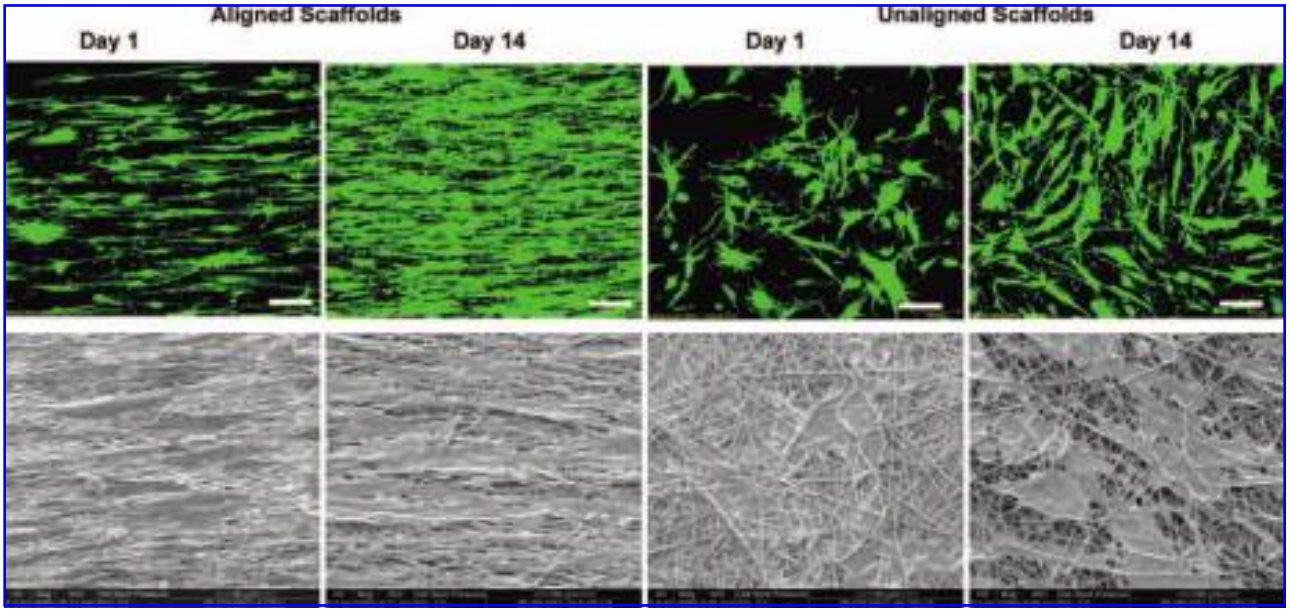

FIG. 3. Effects of nanofiber organization on cell morphology. Top panel: Confocal microscopy of human rotator cuff fibroblasts at day 1 and day 14 (green: live, red: dead), 20×, bar = 100 μm. Bottom panel: Scanning electron micrographs of cells on aligned and unaligned scaffolds at day 1 and day 14, 1000×, bar = 50 μm. The fibroblasts remained viable and grew on both types of substrate over time, with the rotator cuff cells exhibiting phenotypic elongated morphology on the aligned nanofiber scaffolds. Color images available online at www.liebertonline.com/ten.

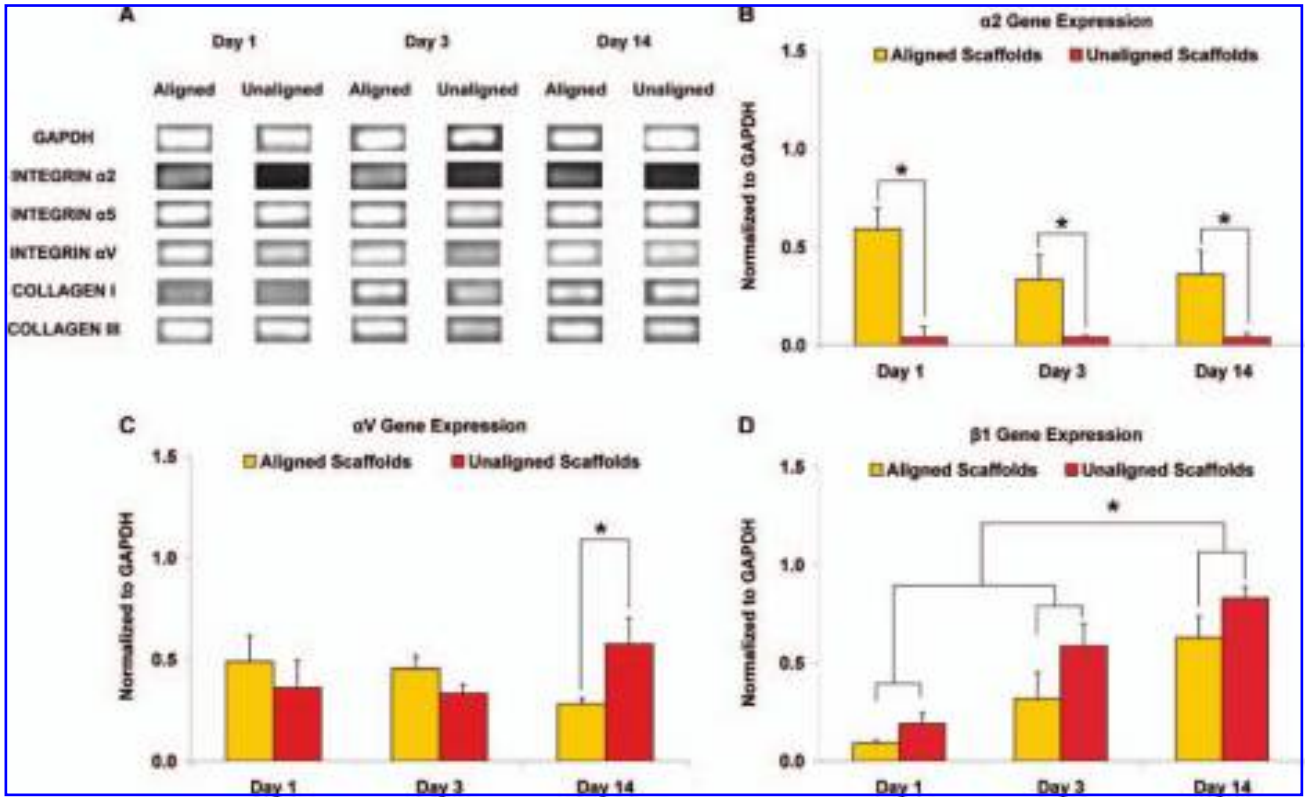

FIG. 4. Gene expression on aligned and unaligned scaffolds over time. (**A**) Fibroblast expression of glyceraldehyde-3-phosphate dehydrogenase (GAPDH), integrins, and type I and type III collagen. (**B**) Expression of the α2 integrin differed significantly on the aligned and unaligned scaffolds at all time points examined ($^*p < 0.05$). (**C**) Expression of αV was significantly higher on the unaligned scaffolds at day 14 ($^*p < 0.05$). (**D**) Although β1 expression did not vary significantly between the two scaffold types, it increased significantly over time ($^*p < 0.05$). Color images available online at www.liebertonline.com/ten.

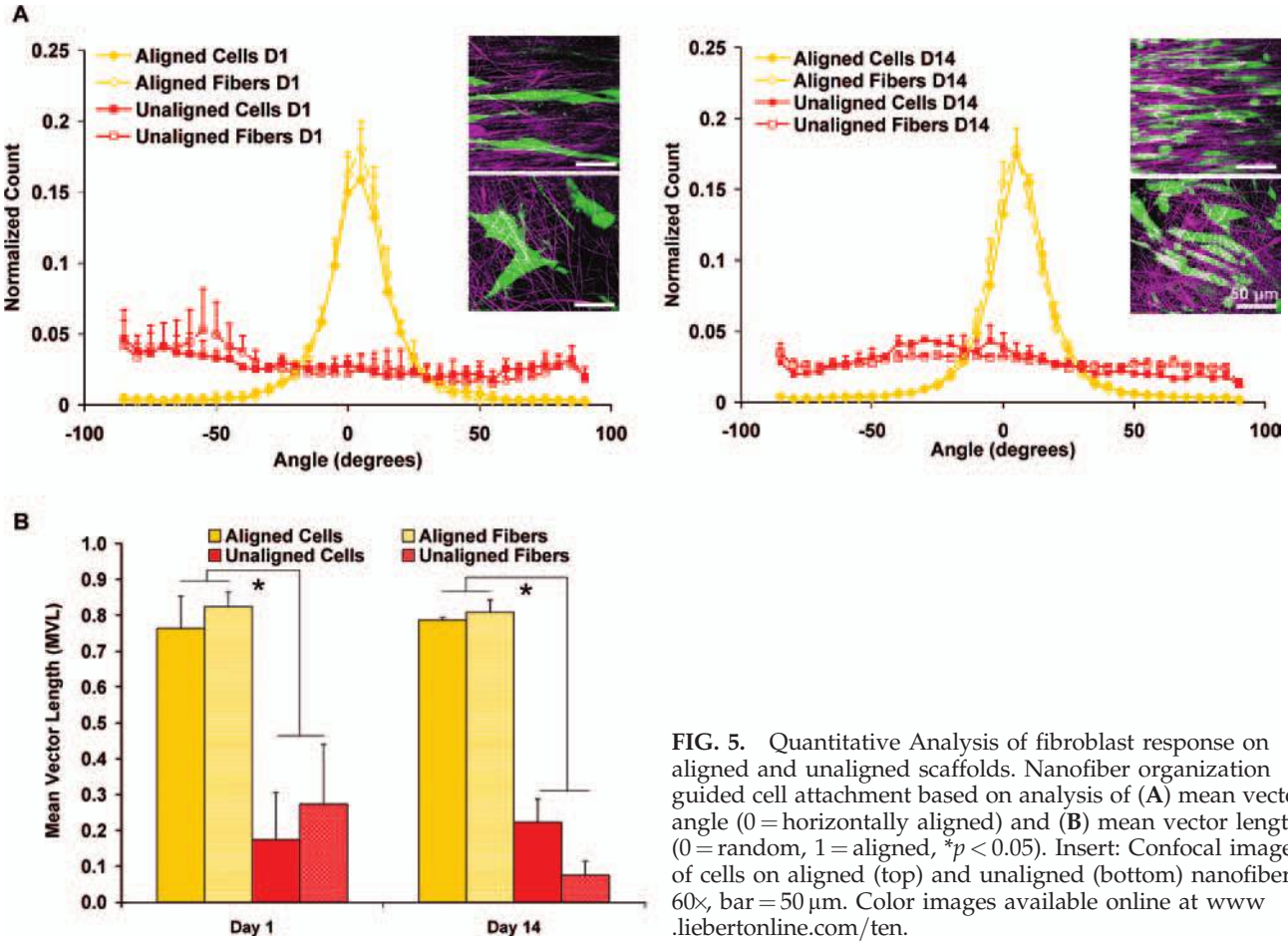

FIG. 5. Quantitative Analysis of fibroblast response on aligned and unaligned scaffolds. Nanofiber organization guided cell attachment based on analysis of (**A**) mean vector angle (0 = horizontally aligned) and (**B**) mean vector length (0 = random, 1 = aligned, $^*p < 0.05$). Insert: Confocal images of cells on aligned (top) and unaligned (bottom) nanofibers, 60×, bar = 50 μm. Color images available online at www.liebertonline.com/ten.

fibroblast-seeded scaffolds did not change significantly over time (Fig. 7).

At all time points examined, the tensile properties of the aligned scaffolds were significantly greater than those of the unaligned scaffolds (Fig. 7, $p < 0.05$), and this trend was consistently observed in the cellular and acellular groups. For the unaligned group, a significant decrease in ultimate tensile strength was detected at day 1, whereas such a decrease was not found until 1 week later in the aligned group (Fig. 7A). The yield strength of the aligned scaffolds decreased significantly at day 1 (Fig. 7C) and continued to drop over time, with a significantly lower yield strength found at day 14 ($p < 0.05$). In contrast, no significant change in yield strength was seen in the unaligned scaffolds over time.

Table 3. Summary of the Alignment Analysis Results

Day 1 (n = 3)	*Mean Angle ± Angular Deviation (°)*
Aligned Cells	4.24 ± 19.73
Aligned Fibers	4.32 ± 17.00
Unaligned Cells	−63.46 ± 37.70
Unaligned Fibers	−55.69 ± 35.97
Day 14 (n = 3)	*Mean Angle ± Angular Deviation (°)*
Aligned Cells	6.19 ± 18.74
Aligned Fibers	4.62 ± 17.78
Unaligned Cells	−19.45 ± 35.93
Unaligned Fibers	−20.84 ± 38.14

Cell and fiber alignment parameters evaluated at 1 and 14 days of culture, represented as mean vector angle (MA: $-90° \le \theta \le 90°$) ± angular deviation (AD: 0–40.5°).

0° indicates horizontal orientation.

Discussion

Our long-term goal is to engineer biomimetic, functional, and integrative scaffold systems for rotator cuff repair and augmentation. This study focuses on the design, characterization, and *in vitro* evaluation of a degradable polymer-based nanofiber scaffold with pre-engineered mechanical properties matching those of native tissue. In this study, the effects of nanofiber organization on the scaffold structural and mechanical properties and the response of primary cells derived from the human rotator cuff tendons were systematically investigated. Additionally, the effects of fibroblast culture on the ability of the nanofiber scaffold to maintain stable mechanical properties were evaluated over time. It is observed that nanofiber organization controls scaffold mechanical properties and is the primary factor guiding the attachment morphology, alignment, integrin expression, and matrix deposition by human rotator cuff fibroblasts. Moreover, although *in vitro* culture resulted in an expected decrease in scaffold mechanical properties with polymer degradation, nanofiber organization modulated these changes. Based on

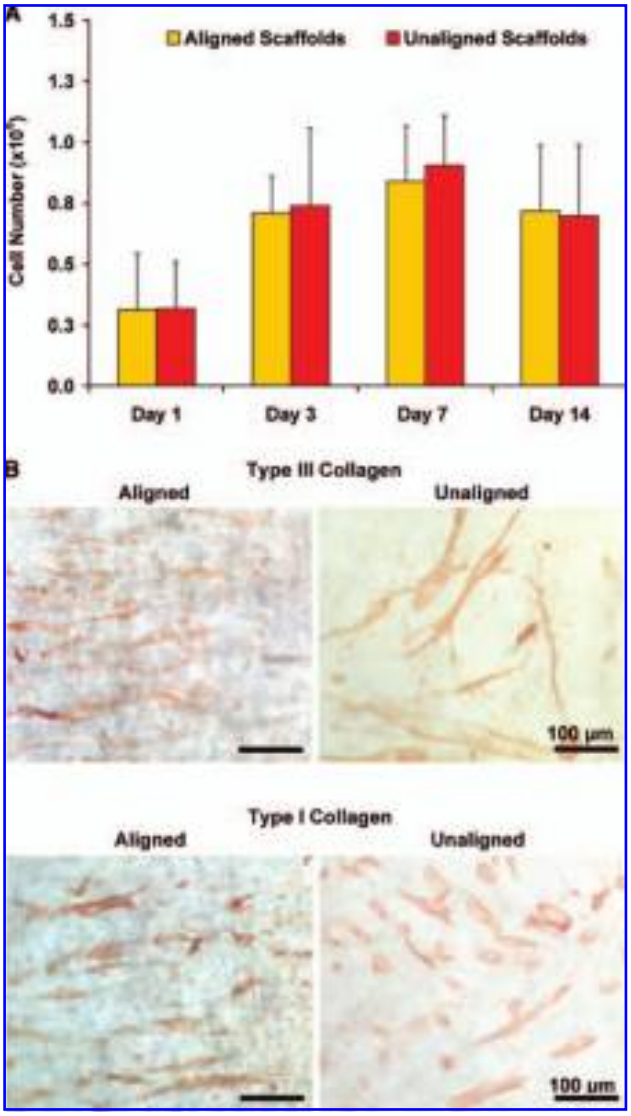

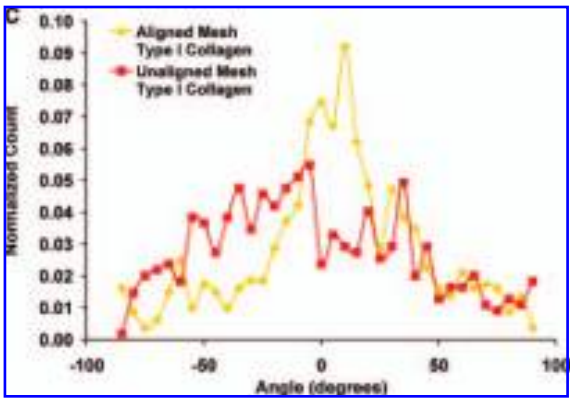

FIG. 6. Cell proliferation and matrix elaboration on aligned and unaligned scaffolds. (**A**) Cells proliferated on both types of scaffolds independent of fiber alignment. (**B**) Immunohistochemical staining for types I and III collagen (day 7, 20×, bar = 100 μm). (**C**) Nanofiber organization also guided matrix production on the nanofiber scaffolds, with an aligned collagen I matrix found on the aligned scaffolds (day 7, mean angle analysis). Color images available online at www.liebertonline.com/ten.

these observations, it is apparent that nanofiber organization exerts significant control over cell response as well as scaffold properties and is a critical graft design parameter for functional rotator cuff repair.

The scaffolds used in this study were pre-designed with similar structural properties (nanofiber diameter, porosity, pore size, permeability); thus, these observed differences in cell response can be attributed to the differences in nanofiber organization (aligned vs unaligned). Qualitative and quantitative analyses revealed that human rotator cuff fibroblasts exhibited a phenotypic morphology and attached preferentially along the nanofiber axis of the aligned scaffolds, whereas only random cell attachment was observed on the unaligned scaffold. These differences were maintained over time, and more importantly, subsequent cell-mediated production of type I and type III collagen also conformed to nanofiber organization.

To further explore this contact guidance phenomena,[44–46] where topography of the biomaterial substrate regulates cell adhesion, expression of key integrins on aligned and unaligned scaffolds were compared over time. Significantly greater α2 expression was consistently detected on the aligned nanofiber scaffolds, whereas αV and β1 expression levels were upregulated on the unaligned scaffolds over time. These observations suggest that human rotator cuff fibroblasts can detect differences in nanofiber alignment during initial attachment, as well as post-adhesion matrix synthesis. Because elevated expression and production of αV and β1 has been associated with healing tendons[47] and ligaments,[48] the differential integrin expression found in this study suggests that cells exposed to the unaligned nanofiber matrix may be primarily undergoing a repair response. In contrast, the physiologically relevant aligned fibers circumvent such a healing response, which may result in disorganized scar tissue formation. Thus the aligned nanofibers directly promote the deposition of a biomimetic collagen matrix instead. The suppression of α2 integrin expression observed on the unaligned scaffolds is also significant. Li *et al.*[23] evaluated fetal bovine chondrocyte response on unaligned nanofiber scaffolds of poly(ε-caprolactone) and also observed that α2 expression was down-regulated when compared with monolayer control. Because α2 complexes with β1 to form the key integrin heterodimer that mediates cell attachment to collagenous matrices,[49–51] its upregulation, only when fibroblasts are cultured on the aligned nanofiber, suggests that this matrix may better mimic the collagen matrix native to the rotator cuff fibroblasts. Although these results are promising, only gene expression was determined in this study. Future work will focus on evaluation of integrin production and the downstream effects of these observed cell responses as a function of nanofiber organization.

Because the nanofiber scaffold is based on degradable polymers, it is important to characterize whether scaffold mechanical properties will be maintained during *in vitro* culture and, moreover, whether cell-mediated matrix production will compensate for the reduction in mechanical properties due to nanofiber degradation. It was observed that, although tensile properties decreased because of hydrolytic degradation of the PLGA nanofibers,[39] its material properties were still within range of those reported for human rotator cuff tendons.[52] This indicates that physiological loading can be sustained while scaffold degradation occurs

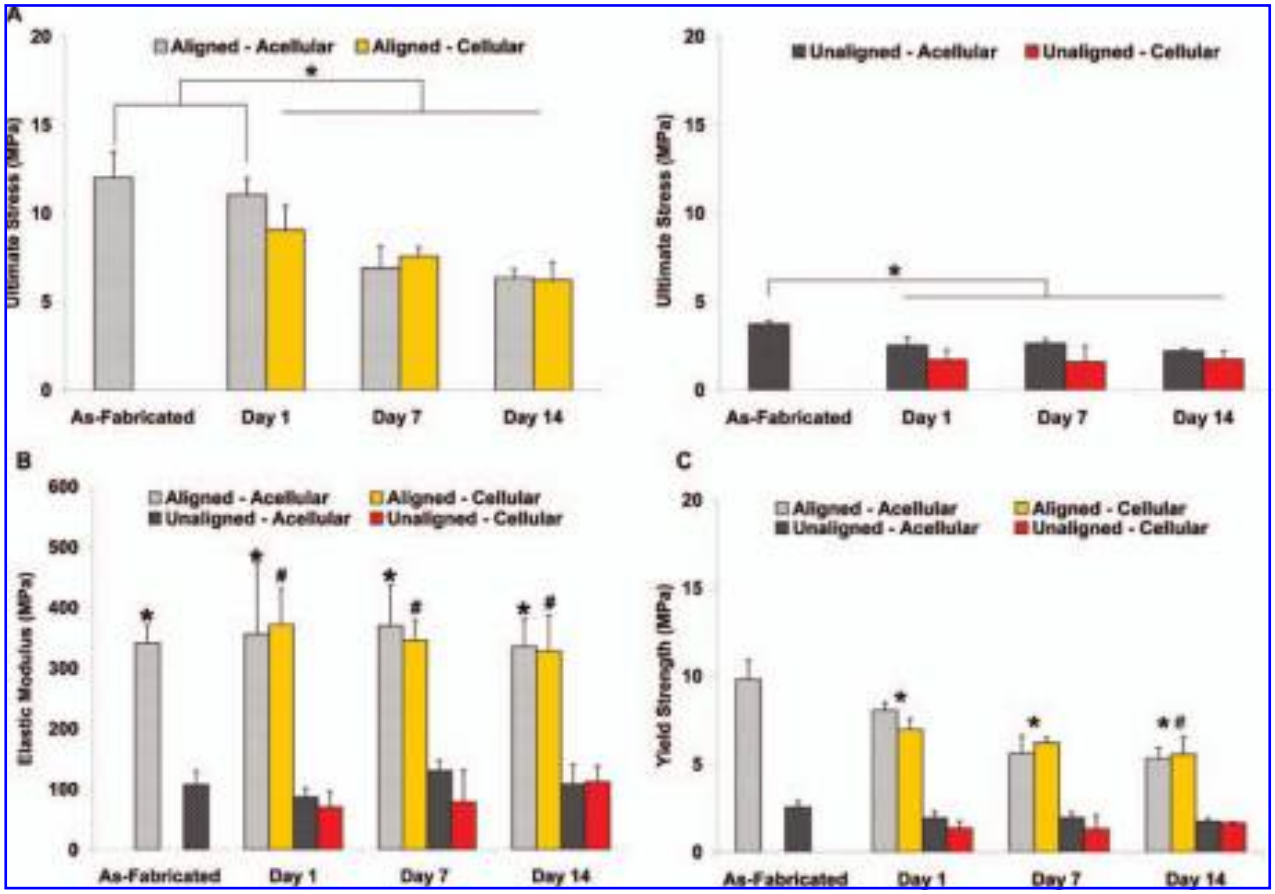

FIG. 7. Effects of *in vitro* culture on scaffold mechanical properties. Mechanical properties of the cell-seeded and acellular scaffolds decreased because of polymer degradation, and aligned scaffolds remained significantly stronger than unaligned scaffolds, (**A**) ultimate tensile strength, $*p < 0.05$; (**B**) elastic modulus, $*p < 0.05$ vs unaligned, and $\#p < 0.05$ vs unaligned cellular scaffolds; and (**C**) yield strength, $*p < 0.05$ for aligned vs as-fabricated aligned scaffolds, and $\#p < 0.05$ day 1 vs day 14. Color images available online at www.liebertonline.com/ten.

and the cell-mediated response is underway. Additionally, the aligned nanofiber scaffolds maintained the as-fabricated tensile mechanical properties longer than the unaligned group. These observations demonstrate that degradation kinetics of the nanofiber scaffolds and associated changes in mechanical properties are dependent on fiber organization. No significant increase in tensile properties with fibroblast culture was observed, which is probably due to the relatively short culturing time evaluated in this study. Cell-mediated increases in mechanical properties were reported only after more than 2 months of *in vitro* culture.[21] The effects of long-term culture on scaffold mechanical properties will be investigated in future studies.

In this study, the human rotator cuff fibroblasts proliferated over time on both types of nanofiber scaffolds, with no significant differences observed between the scaffold groups. These results corroborate previous studies that also reported minimal effect on cell proliferation due to nanofiber organization.[21,24] Although fiber organization differed, types I and III collagen deposition were observed on the aligned and unaligned scaffolds. While total collagen content was not quantified in this study, fiber architecture has been reported to have minimal effect on collagen production for bovine mesenchymal stem cells and meniscal fibrochondrocytes cultured on aligned and unaligned poly(ε-caprolactone) nanofiber scaffolds.[21] Furthermore, collagen synthesis by human ligament fibroblasts grown on aligned polyurethane nanofiber scaffolds was significantly greater after being subjected to tensile loading.[24] It is likely that mechanical stimulation and fiber organization may be coupled to promote overall collagen production over time and in turn improve cuff healing and long-term clinical outcome.

The PLGA nanofiber-based scaffold represents a promising system for functional repair and augmentation of rotator cuff tendons. In this study, the tensile modulus of the unaligned and aligned scaffolds averaged 107 MPa and 341 MPa, respectively, with mean ultimate tensile strength ranging from 3.7 to 12.0 MPa. In addition to possessing physiologically relevant mechanical properties and fiber diameter approximating that of native collagen matrix, the nanofiber scaffold reported here exhibits structural properties that are optimal for soft tissue repair, including porosity greater than 80% and high permeability, which can facilitate nutrient transport and promote cell viability and tissue growth *in vitro* and *in vivo*. The permeability of the scaffold is also within range of those reported for musculoskeletal

tissues.[37,53–56] Moreover, the observed differences in cell response to aligned or unaligned scaffolds and the resultant matrix properties can be readily exploited for functional repair of rotator cuff injuries and the formation of complex tissues. A distinct advantage of the nanofiber scaffold is that matrix anisotropy can be incorporated into scaffold design by varying nanofiber organization and alignment. This is especially desirable for tendon repair or regeneration, because scaffolds with controlled matrix anisotropy can be fabricated to recapitulate the inherent structure–function relationship of the rotator cuff tendons. When Itoi *et al.*[52] evaluated the tensile mechanical properties of the human supraspinatus tendon at the anterior, middle, and posterior regions of the tendon, region-dependent changes in elastic modulus and ultimate tensile stress were observed. Specifically, the magnitude of the elastic modulus ranged from 50 MPa to 170 Mpa when progressing from the posterior to the anterior region, whereas the ultimate tensile strength ranged from 4.1 MPa to 16.5 MPa from the posterior to the superficial tendon region. Moreover, collagen organization and alignment are reported to play a role in reducing stress concentration at the supraspinatus tendon-to-bone insertion.[57] Therefore, by controlling nanofiber organization (alignment or layering), polymer composition, and molecular weight, nanofiber scaffolds with biomimetic collagen alignment and region-dependent mechanical properties can be readily engineered and used for rotator cuff repair and augmentation.

Conclusion

This study focused on the design, characterization, and systematic *in vitro* evaluation of a novel biomimetic, biodegradable, nanofiber-based scaffold for functional rotator cuff repair. It was found that nanofiber organization has a significant effect on human rotator cuff fibroblast response, with the structural anisotropy of the aligned and isotropy of the unaligned scaffold directly guiding cell attachment, integrin expression, and matrix deposition. Controlled cell response resulted in a biomimetic matrix for rotator cuff repair on the aligned nanofiber scaffold, and physiologically relevant scaffold mechanical properties were maintained *in vitro*. The findings of this study demonstrate that the novel nanofiber scaffold has significant potential for tendon regeneration and represents a functional tissue-engineering solution for rotator cuff repair. Future studies will focus on scaffold optimization and *in vivo* evaluation of the nanofiber system for rotator cuff repair and augmentation.

Acknowledgments

The authors would like to thank Anthony Labissiere at the Hospital for Special Surgery for assistance with SEM analysis and Gregory M. Fomovsky, M.S., and Jeffrey W. Holmes, M.D., Ph.D., at the University of Virginia for assistance with circular statistical analysis. We also thank Michael B. Albro, M.S., and Gerard A. Ateshian, Ph.D., at Columbia University for assistance with permeability measurements. This study was supported by the National Institutes of Health, National Institute of Arthritis and Musculoskeletal and Skin Diseases (AR0524202-01, HHL/WNL) and the National Science Foundation (Graduate Fellowship, GK-12 0338329, KLM).

References

1. Vitale, M. A., Vitale, M. G., Zivin, J. G., Braman, J. P., Bigliani, L. U., and Flatow, E. L. Rotator cuff repair: an analysis of utility scores and cost-effectiveness. J Shoulder Elbow Surg **16,** 181, 2007.
2. Codman, E. The Shoulder, Rupture of the Supraspinatus Tendon and Other Lesions In or About the Subacromial Bursa. Boston: Thomas Todd, 193).
3. Yamanaka, K. and Matsumoto, T. The joint side tear of the rotator cuff. A followup study by arthrography. Clin Orthop Relat Res **68,** 1994.
4. Dejardin, L. M., Arnoczky, S. P., Ewers, B. J., Haut, R. C., and Clarke, R. B. Tissue- engineered rotator cuff tendon using porcine small intestine submucosa. Histologic and mechanical evaluation in dogs. Am J Sports Med **29,** 175, 2001.
5. Galatz, L. M., Ball, C. M., Teefey, S. A., Middleton, W. D., and Yamaguchi, K. The outcome and repair integrity of completely arthroscopically repaired large and massive rotator cuff tears. J Bone Joint Surg Am **86-A,** 219, 2004.
6. Gazielly, D. F., Gleyze, P., and Montagnon, C. Functional and anatomical results after rotator cuff repair. Clin Orthop Relat Res **43,** 1994.
7. Gartsman, G. M. Massive, irreparable tears of the rotator cuff. Results of operative debridement and subacromial decompression. J Bone Joint Surg Am **79,** 715, 1997.
8. Rokito, A. S., Zuckerman, J. D., Gallagher, M. A., and Cuomo, F. Strength after surgical repair of the rotator cuff. J Shoulder Elbow Surg **5,** 12, 1996.
9. DeOrio, J. K. and Cofield, R. H. Results of a second attempt at surgical repair of a failed initial rotator-cuff repair. J Bone Joint Surg Am **66,** 563, 1984.
10. Gerber, C., Schneeberger, A. G., Perren, S. M., and Nyffeler, R. W. Experimental rotator cuff repair. A preliminary study. J Bone Joint Surg Am **81,** 1281, 1999.
11. Post, M. Rotator cuff repair with carbon filament. A preliminary report of five cases. Clin Orthop Relat Res **154,** 1985.
12. Ozaki, J., Fujimoto, S., Masuhara, K., Tamai, S., and Yoshimoto, S. Reconstruction of chronic massive rotator cuff tears with synthetic materials. Clin Orthop Relat Res 173 1986.
13. Schlegel, T. F., Hawkins, R. J., Lewis, C. W., Motta, T., and Turner, A. S. The effects of augmentation with swine small intestine submucosa on tendon healing under tension: histologic and mechanical evaluations in sheep. Am J Sports Med **34,** 275, 2006.
14. Badylak, S. F. The extracellular matrix as a scaffold for tissue reconstruction. Semin Cell Dev Biol **13,** 377, 2002.
15. Derwin, K. A., Baker, A. R., Spragg, R. K., Leigh, D. R., and Iannotti, J. P. Commercial extracellular matrix scaffolds for rotator cuff tendon repair. Biomechanical, biochemical, and cellular properties. J Bone Joint Surg Am **88,** 2665, 2006.
16. Iannotti, J. P., Codsi, M. J., Kwon, Y. W., Derwin, K., Ciccone, J., and Brems, J. J. Porcine small intestine submucosa augmentation of surgical repair of chronic two-tendon rotator cuff tears. A randomized, controlled trial. J Bone Joint Surg Am **88,** 1238, 2006.
17. Sclamberg, S. G., Tibone, J. E., Itamura, J. M., and Kasraeian, S. Six-month magnetic resonance imaging follow-up of large and massive rotator cuff repairs reinforced with porcine small intestinal submucosa. J Shoulder Elbow Surg **13,** 538, 2004.

18. Coons, D. A. and Alan, B. F. Tendon graft substitutes-rotator cuff patches. Sports Med Arthrosc **14,** 185, 2006.
19. Yoshimoto, H., Shin, Y. M., Terai, H., and Vacanti, J. P. A biodegradable nanofiber scaffold by electrospinning and its potential for bone tissue engineering. Biomaterials **24,** 2077, 2003.
20. Garreta, E., Gasset, D., Semino, C., and Borros, S. Fabrication of a three-dimensional nanostructured biomaterial for tissue engineering of bone. Biomol Eng **24,** 75, 2007.
21. Baker, B. M. and Mauck, R. L. The effect of nanofiber alignment on the maturation of engineered meniscus constructs. Biomaterials **28,** 1967, 2007.
22. Nerurkar, N. L., Elliott, D. M., and Mauck, R. L. Mechanics of oriented electrospun nanofibrous scaffolds for annulus fibrosus tissue engineering. J Orthop Res **25,** 1018, 2007.
23. Li, W. J., Danielson, K. G., Alexander, P. G., and Tuan, R. S. Biological response of chondrocytes cultured in three-dimensional nanofibrous poly(epsilon-caprolactone) scaffolds. J Biomed Mater Res A **67,** 1105, 2003.
24. Lee, C. H., Shin, H. J., Cho, I. H., Kang, Y. M., Kim, I. A., Park, K. D., and Shin, J. W. Nanofiber alignment and direction of mechanical strain affect the ECM production of human ACL fibroblast. Biomaterials **26,** 1261, 2005.
25. Bashur, C. A., Dahlgren, L. A., and Goldstein, A. S. Effect of fiber diameter and orientation on fibroblast morphology and proliferation on electrospun poly(D,L-lactic-co-glycolic acid) meshes. Biomaterials **27,** 5681, 2006.
26. Li, W. J., Laurencin, C. T., Caterson, E. J., Tuan, R. S., and Ko, F. K. Electrospun nanofibrous structure: a novel scaffold for tissue engineering. J Biomed Mater Res **60,** 613, 2002.
27. Ma, Z., Kotaki, M., Inai, R., and Ramakrishna, S. Potential of nanofiber matrix as tissue- engineering scaffolds. Tissue Eng **11,** 101, 2005.
28. Christenson, E. M., Anseth, K. S., van den Beucken, J. J., Chan, C. K., Ercan, B., Jansen, J. A., Laurencin, C. T., Li, W. J., Murugan, R., Nair, L. S., Ramakrishna, S., Tuan, R. S., Webster, T. J., and Mikos, A. G. Nanobiomaterial applications in orthopedics. J Orthop Res 25, 11 2007.
29. Pham, Q. P., Sharma, U., and Mikos, A. G. Electrospinning of polymeric nanofibers for tissue engineering applications: a review. Tissue Eng **12,** 1197, 2006.
30. Li, W. J., Mauck, R. L., Cooper, J. A., Yuan, X., and Tuan, R. S. Engineering controllable anisotropy in electrospun biodegradable nanofibrous scaffolds for musculoskeletal tissue engineering. J Biomech **40,** 1686, 2007.
31. Murugan, R. and Ramakrishna, S. Design strategies of tissue engineering scaffolds with controlled fiber orientation. Tissue Eng **13,** 1845, 2007.
32. Pham, Q. P., Sharma, U., and Mikos, A. G. Electrospun poly(epsilon-caprolactone) microfiber and multilayer nanofiber/microfiber scaffolds: characterization of scaffolds and measurement of cellular infiltration. Biomacromolecules **7,** 2796, 2006.
33. Formhals, A. Process and Apparatus for Preparing Artificial Threads. (Patent #: 1,975,504). 1934.
34. Reneker, D. H. and Chun, I. Nanometre diameter fibres of polymer, produced by electrospinning. Nanotechnology **7,** 216, 1996.
35. Matthews, J. A., Wnek, G. E., Simpson, D. G., and Bowlin, G. L. Electrospinning of collagen nanofibers. Biomacromolecules **3,** 232, 2002.
36. Lu, H. H., El Amin, S. F., Scott, K. D., and Laurencin, C. T. Three-dimensional, bioactive, biodegradable, polymer-bioactive glass composite scaffolds with improved mechanical properties support collagen synthesis and mineralization of human osteoblast-like cells *in vitro.* J Biomed Mater Res **64A,** 465, 2003.
37. Albro, M. B., Chahine, N. O., Caligaris, M., Wei, V. I., Likhitpanichkul, M., Ng, K. W., Hung, C. T., and Ateshian, G. A. Osmotic loading of spherical gels: a biomimetic study of hindered transport in the cell protoplasm. J Biomech Eng **129,** 503, 2007.
38. Weiss, J. A. and Maakestad, B. J. Permeability of human medial collateral ligament in compression transverse to the collagen fiber direction. J Biomech **39,** 276, 2006.
39. Lu, H. H., Cooper, J. A., Jr., Manuel, S., Freeman, J. W., Attawia, M. A., Ko, F. K., and Laurencin, C. T. Anterior cruciate ligament regeneration using braided biodegradable scaffolds: *in vitro* optimization studies. Biomaterials **26,** 4805, 2005.
40. Spalazzi, J. P., Vyner, M. C., Jacobs, M. T., Moffat, K. L., and Lu, H. H. Mechanoactive scaffold induces tendon remodelling and expression of fibrocartilage markers. Clin Orthop Rel Res 466(8):1528, 2008.
41. Karnovsky, M. J. A formaldehyde-glutaraldehyde fixative of high osmolarity for use in electron microscopy. J Cell Biol **27,** 137A 1965.
42. Costa, K. D., Lee, E. J., and Holmes, J. W. Creating alignment and anisotropy in engineered heart tissue: role of boundary conditions in a model three-dimensional culture system. Tissue Eng **9,** 567, 2003.
43. Thomopoulos, S., Fomovsky, G. M., Chandran, P. L., and Holmes, J. W. Collagen fiber alignment does not explain mechanical anisotropy in fibroblast populated collagen gels. J Biomech Eng **129,** 642, 2007.
44. Singhvi, R., Kumar, A., Lopez, G. P., Stephanopoulos, G. N., Wang, D. I., Whitesides, G. M., and Ingber, D. E. Engineering cell shape and function. Science **264,** 696, 1994.
45. Clark, P., Connolly, P., Curtis, A. S., Dow, J. A., and Wilkinson, C. D. Cell guidance by ultrafine topography *in vitro*. J Cell Sci **99 (Pt 1),** 73, 1991.
46. Wang, J. H., Jia, F., Gilbert, T. W., and Woo, S. L. Cell orientation determines the alignment of cell-produced collagenous matrix. J Biomech **36,** 97, 2003.
47. Harwood, F. L., Monosov, A. Z., Goomer, R. S., Gelberman, R. H., Winters, S. C., Silva, M. J., and Amiel, D. Integrin expression is upregulated during early healing in a canine intrasynovial flexor tendon repair and controlled passive motion model. Connect Tissue Res **39,** 309, 1998.
48. Schreck, P. J., Kitabayashi, L. R., Amiel, D., Akeson, W. H., and Woods, V. L., Jr. Integrin display increases in the wounded rabbit medial collateral ligament but not the wounded anterior cruciate ligament. J Orthop Res **13,** 174, 1995.
49. Staatz, W. D., Fok, K. F., Zutter, M. M., Adams, S. P., Rodriguez, B. A., and Santoro, S. A. Identification of a tetrapeptide recognition sequence for the alpha 2 beta 1 integrin in collagen. J BiolChem. **266,** 7363, 1991.
50. Hynes, R. O. Integrins: bidirectional, allosteric signaling machines. Cell **110,** 673, 2002.
51. Garcia, A. J. Get a grip: integrins in cell-biomaterial interactions. Biomaterials 26, 7525 2005.
52. Itoi, E., Berglund, L. J., Grabowski, J. J., Schultz, F. M., Growney, E. S., Morrey, B. F., and An, K. N. Tensile properties of the supraspinatus tendon. J Orthop Res **13,** 578, 1995.
53. Joshi, M. D., Suh, J. K., Marui, T., and Woo, S. L. Interspecies variation of compressive biomechanical properties of the meniscus. J Biomed Mater Res **29,** 823, 1995.
54. Iatridis, J. C., Setton, L. A., Foster, R. J., Rawlins, B. A., Weidenbaum, M., and Mow, V. C. Degeneration affects the

anisotropic and nonlinear behaviors of human anulus fibrosus in compression. J Biomech **31,** 535, 1998.
55. LeRoux, M. A. and Setton, L. A. Experimental and biphasic FEM determinations of the material properties and hydraulic permeability of the meniscus in tension. J Biomech Eng **124,** 315, 2002.
56. Yin, L. and Elliott, D. M. A biphasic and transversely isotropic mechanical model for tendon: application to mouse tail fascicles in uniaxial tension. J Biomech **37,** 907, 2004.
57. Thomopoulos, S., Williams, G. R., Gimbel J.A., Favata, M., and Soslowsky, L. J. Variations of biomechanical, structural, and compositional properties along the tendon to bone insertion site. J Orthop Res **21,** 413, 2003.

Address reprint requests to:
Helen H. Lu, Ph.D.
Department of Biomedical Engineering
Columbia University
1210 Amsterdam Avenue
351 Engineering Terrace, MC 8904
New York, NY 10027

E-mail: hl2052@columbia.edu

Received: January 5, 2008
Accepted: May 9, 2008